A&A 444, 265–274 (2005)
DOI: 10.1051/0004-6361:20053604

Astronomy & Astrophysics

DOT tomography of the solar atmosphere

V. Analysis of a surge from AR10486

K. Tziotziou[1], G. Tsiropoula[2], and P. Sütterlin[1]

[1] Sterrekundig Instituut, Utrecht University, Postbus 80 000, 3508 TA Utrecht, The Netherlands
e-mail: [k.tziotziou;p.suetterlin]@astro.uu.nl
[2] National Observatory of Athens, Institute for Space Applications and Remote Sensing, Lofos Koufos, 15236 Palea Penteli, Greece
e-mail: georgia@space.noa.gr

Received 9 June 2005 / Accepted 9 August 2005

ABSTRACT

We present an analysis of high temporal and spatial resolution CaII H chromospheric limb observations obtained with the Dutch Open Telescope (DOT). We focus on a solar surge observed both by the DOT in CaII H and the Transition Region and Coronal Explorer (TRACE) satellite in the 195 Å and 1600 Å passbands. The surge is observed in active region AR10486 located near the solar limb, a region which two hours later produced the largest X-flare ever recorded. It consists of relatively cold gas of about 10^4–10^5 K. In TRACE images the surge is followed for almost 2.5 h, shrinking and expanding at the same location several times. From DOT images we find outward propagating intensity disturbances, with velocities higher than 50 km s^{-1}, indicative of upward material motion. The latter is also suggested by the good correlation between the DOT and TRACE surge apparent height curves, their apparent time delay and a phase difference analysis. A spectral wavelet analysis of the brightness variations within and along the surge shows a predominant period of ∼6 min, the first ever reported for this kind of structures. Magnetic reconnection at the bottom of the surge as its driving mechanism is suggested by the observed inverted "Y" shape configuration and is further supported by a phase difference analysis.

Key words. Sun: chromosphere – Sun: transition region – Sun: activity – methods: data analysis

1. Introduction

The solar chromosphere is a highly inhomogeneous region, full of structures of different intensities, shapes and sizes. In active regions gas ejections are regularly observed and manifest themselves as moving prominences on the limb. One type of such ejections is a "surge", which typically has the form of a straight or slightly curved spike. Hα surges have been studied for over 50 years (see Roy 1973a,b, and references therein). They typically last 10–20 min, reach heights of up to 200 Mm, with peak velocities of 50–200 km s^{-1}, and then fade or fall back to the chromosphere, apparently along the trajectory of ascent (Svestka 1976; Tandberg-Hanssen 1977; Schmieder et al. 1994). They are evolving over a small dark mound-like region forming an inverted "Y" configuration. Kurokawa & Kawai (1993) suggested that this shape can be explained by magnetic reconnection. Observations show that surges are usually associated with small, changing satellite sunspots which represent islands of polarity reversal (Rust 1968; Canfield et al. 1996) situated close to the edges of sunspot penumbrae, or with newly magnetic flux emergence in close proximity to an opposite polarity pre-existing flux (Yoshimura et al. 2003). Such observations provide additional evidence in support of reconnection and several reconnection models have already been proposed (Canfield et al. 1996; Yokohama & Shibata 1996).

Several other types of structure are observed in the quiet and active chromosphere. The network boundaries, which outline the photospheric supergranule cells, are the locus of most of the quiet chromosphere fine structures, known as mottles when seen on the disk. Their most likely limb counterparts are spicules. In active regions bright and dark elongated structures are observed that are similar to mottles, although usually more extended. These are referred to as fibrils. Fibrils give the filamentary appearance of sunspots penumbrae and superpenumbrae. According to Foukal (1971) mottles and fibrils are similar structures, the latter being more inclined to the normal following the topology of the local magnetic field.

Apart from the differences in scales (length, time and velocity) there are strong similarities between a mottle (or spicule) and a surge. Both have a strong recurrence tendency repeating themselves at apparently the same location. Moreover, both carry the signature of the underlying magnetic field and are thought to be associated with magnetic reconnection. It is thus possible that they are the manifestation of the same phenomenon occurring on different scales. In this context, detailed study of the dynamical evolution of individual structures is

important in understanding the characteristics of the magnetic field and the nature of the physical processes which produce them.

In Tziotziou et al. (2004) we applied a wavelet analysis and found that intensity and velocity variations in dark mottles in a quiet region display a dominant period of ∼5–6 min. The same behaviour we found for fibrils in the periphery of a plage. Five to six minute oscillations in dark fibrils have also been reported by De Pontieu et al. (2003), who, furthermore, suggested p-modes as their driver. To our knowledge no observations of any kind of periodicities in surges have been reported so far.

In this paper we discuss Ca II H images containing active region AR10486 near the solar limb obtained by the Dutch Open Telescope (DOT). We focus on a surge which is present with remarkable clarity in these DOT images and simultaneously in UV and EUV images obtained by the Transition Region and Coronal Explorer (TRACE). In particular, we study its temporal behaviour in sequel to the work of Tziotziou et al. (2004) for mottles and fibrils.

2. Observations and data reduction

The observations used in this study were obtained on November 4, 2003 with the DOT (Rutten et al. 2004a). Image sequences were taken between 16:21:20 and 16:47:35 UT in the Ca II H passband. The filter was tuned to the line core at 3968 Å and has a bandwidth of 1.35 Å. Speckle bursts of 100 frames each were taken at a rate of 6 frames s^{-1}. The individual frames were speckle reconstructed (see Rutten et al. 2004a, for details), yielding one reconstructed image per burst, and these images are then carefully aligned in time. The final time sequence consists of 63 frames of 1140 pixels × 910 pixels with 0.071″/pixel and a 25 s cadence. TRACE (Handy et al. 1999) observed the same region on November 4, 2003 between 14:30:12 and 18:29:43 UT in the 1600 Å and 195 Å passbands. The respective cadences are 39 ± 9 s and 43 ± 13 s, but there are some gaps of several minutes in the observations, however not during the DOT time sequence. The TRACE images measure 768 pixels × 768 pixels at 1 pixel equal to 0.5″. The TRACE data have been corrected for dark current, a CCD readout pedestal value of 87 Data Numbers (DN), hot pixels and radiation spikes due to cosmic rays, and have been co-aligned by cross-correlation to correct for solar rotation and spacecraft pointing jitter. For co-alignment subsequences of 20 frames were aligned to the last previously aligned frame. A 5 × 5 pixel boxcar running average over nine of these coarsely aligned frames was produced, and each frame was aligned to this running average. TRACE images were used for comparison with DOT images. TRACE–DOT co-alignment was done by choosing corresponding images observed almost at the same time (∼16:40 UT) and using standard IDL solar software based on recognition of solar features.

3. Description of the observations

The present DOT Ca II H observations are among the best high-resolution observations of the solar limb ever recorded.

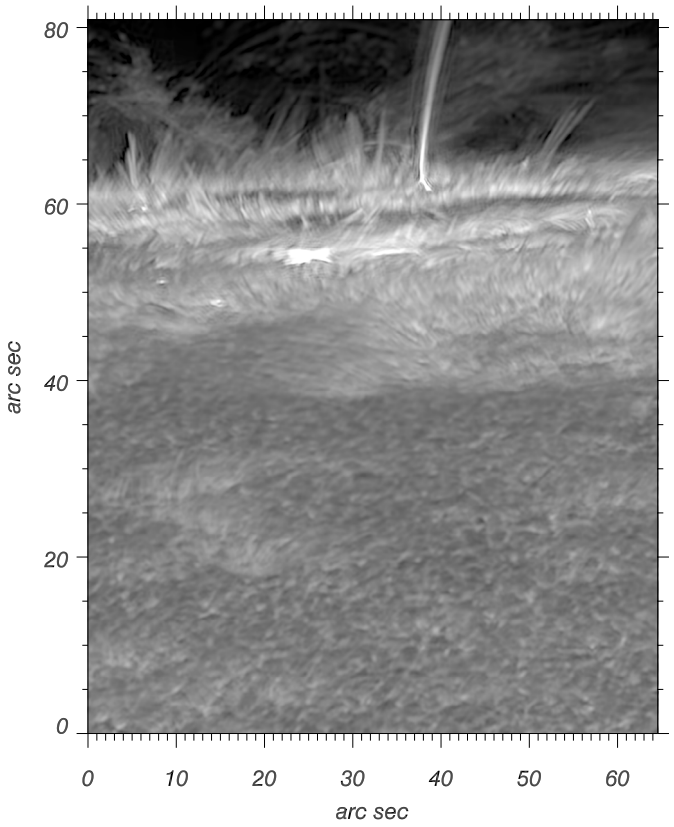

Fig. 1. A sample DOT Ca II H filtergram showing the surge studied in this paper. The dark pancake structures near the limb are sunspots. The bright large-scale cellular pattern at the bottom of the image is the chromospheric network, while reverse granulation is seen in the internetwork. Numerous jet-like structures are clearly visible on the limb in addition to the surge.

Figure 1 shows an example image of these observations. The lower part of the image shows quiet Sun, with the chromospheric network as a bright large-scale cellular pattern and reversed granulation (Rutten et al. 2004b; Leenaarts & Wedemeyer-Böhm 2005) in the internetwork. Several round or elongated, mainly bright but also dark structures are found all over the quiet solar region, usually funning out from the network in a bushlike arrangement. They display substantial changes both in brightness and length with time. Many reappear at the same location after fading. Active region AR10486 is clearly visible at the top of Fig. 1. It produced the largest X-flare ever recorded starting around 19:36 UT, almost three hours after the start of DOT observations. The large, dark structures near the limb are sunspot umbrae. Around their periphery a fairly regular penumbral structure is seen consisting of numerous bright fibrils, packed close together and imaged here with remarkable clarity. The lower ends of the fibrils are more or less at right angles to the local umbrae, although some of them form small loops (see Fig. 1 between x = 50″–60″ and y = 57″–60″). These fibrils are very similar to spicules in appearance and it is impossible to distinguish whether structures seen exactly at the limb are the one structure or the other. Individual fibrils seem to have heights of ∼2″–3″ (probably because only their lower parts are visible) and are very narrow,

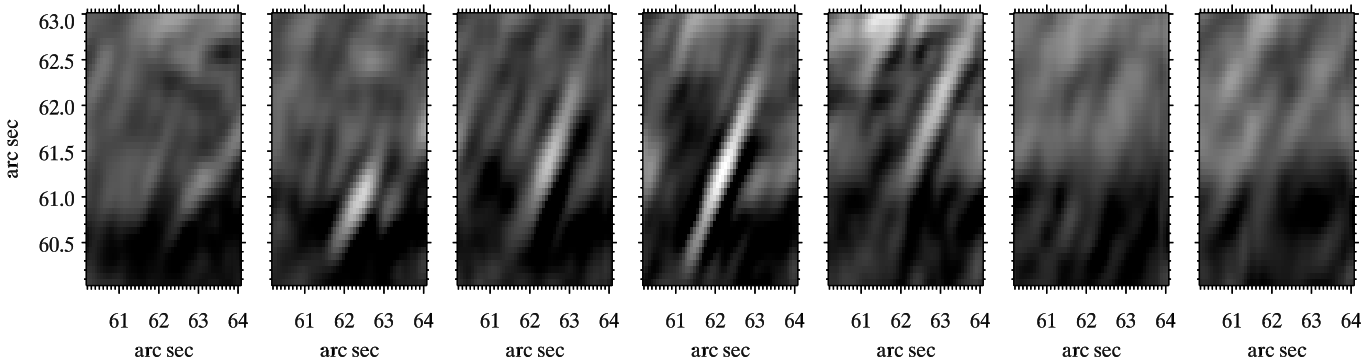

Fig. 2. Temporal evolution of a fibril observed with DOT. The coordinates in the x and y axes correspond to the same coordinates of Fig. 1. The presented sequence starts at 16:22:35 UT and the time cadence is 75 s.

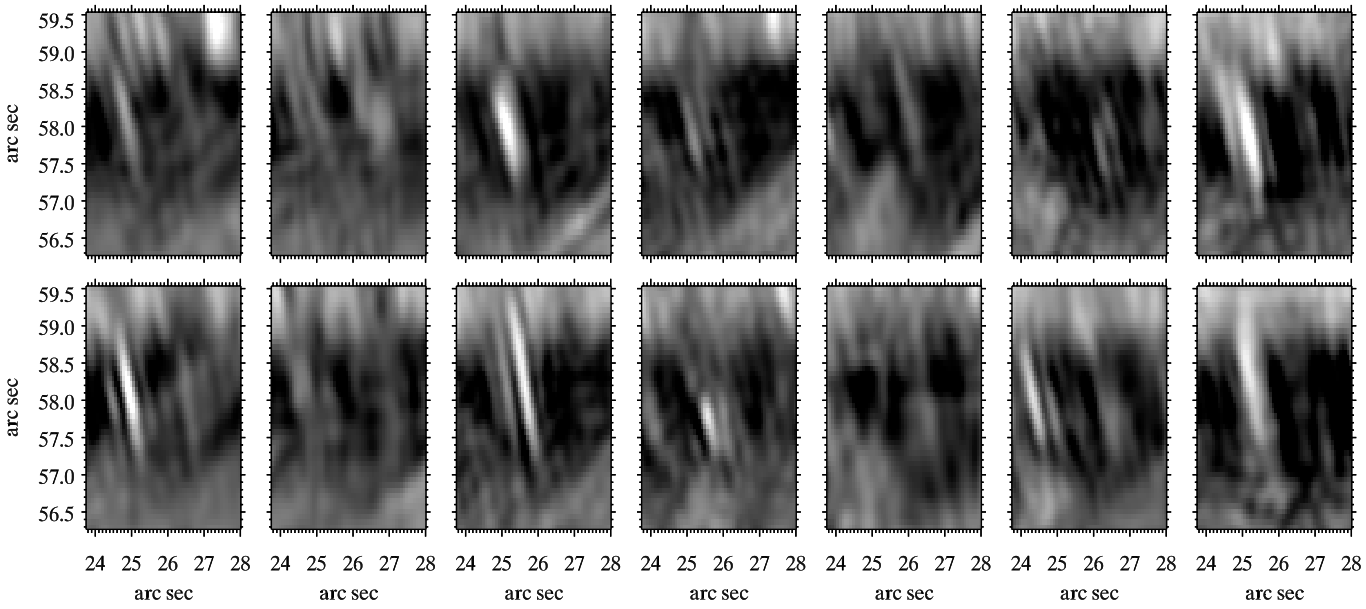

Fig. 3. Two fibrils observed with DOT showing recurrent behaviour. The coordinates in the x and y axes correspond to the same coordinates of Fig. 1. The presented sequence starts at 16:25:55 UT (*top left image*) and the time cadence is 75 s (time runs from top to bottom and from left to right).

often appearing to be less than 0.5″ in width. When they are not overlapped by other structures, it is easy to follow their evolution, which is quite complex. Some of them, despite changes in brightness, size and shape, are observed to persist for the whole time sequence. Such an example is shown in Fig. 2. The fibril begins as a short bright structure and then elongates to its maximum length in the fourth panel. It then dims, but remains visible until the end of the sequence. Other structures reappear several times with few-minute periodicities (see Fig. 3 for a characteristic example).

The solar limb is protruded by a myriad of bright jets with footpoints located in front or behind the limb. Among them is the remarkable surge analysed in this paper. The surge, already in progress when the DOT observations started, appears in emission and is a stand-alone structure. It extends upward beyond the DOT field of view with a projected extent of more than 14 Mm. Its base is sometimes obscured by fluxtubes, and it remains stable throughout the 26-min duration of the DOT sequence. It has the form of a slightly curved jet and fits the "Eiffel tower" description of Kurokawa & Kawai (1993): it evolves over a small dark mound-like region forming an inverted "Y" configuration. These authors suggest that this shape can be explained by magnetic reconnection. Since the active region is near the limb, it is not possible to inspect it on magnetograms recorded by the Michelson Doppler Imager (MDI) onboard the Solar Heliospheric Observatory (SOHO). However, MDI magnetograms of the previous days show that there were ample evolving bipolar fields in the area where the surge appears. It is thus very likely that the surge is produced by reconnection.

In Fig. 4 contours of a DOT image have been overplotted on TRACE 1600 Å (top) and 195 Å (bottom) images taken at nearly the same time. The first samples plasma at low temperatures ($\sim 10^4$ K), but also including C IV emission from plasma of $\sim 10^5$ K. The lower image samples plasma at temperatures of $\sim 1.4 \times 10^6$ K. The surge appears in emission at 1600 Å, as in Ca II H. From this we conclude that the surge consists of relatively cold gas of about 10^4–10^5 K. On the other hand,

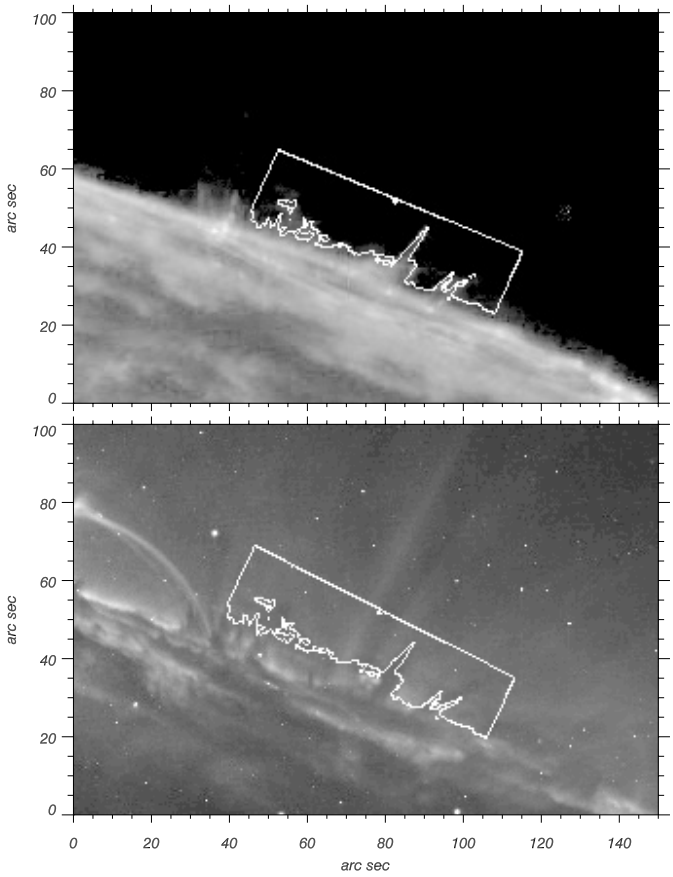

Fig. 4. TRACE 1600 Å image (*top*) and 195 Å image (*bottom*) with overplotted white contours of the DOT Ca II H data.

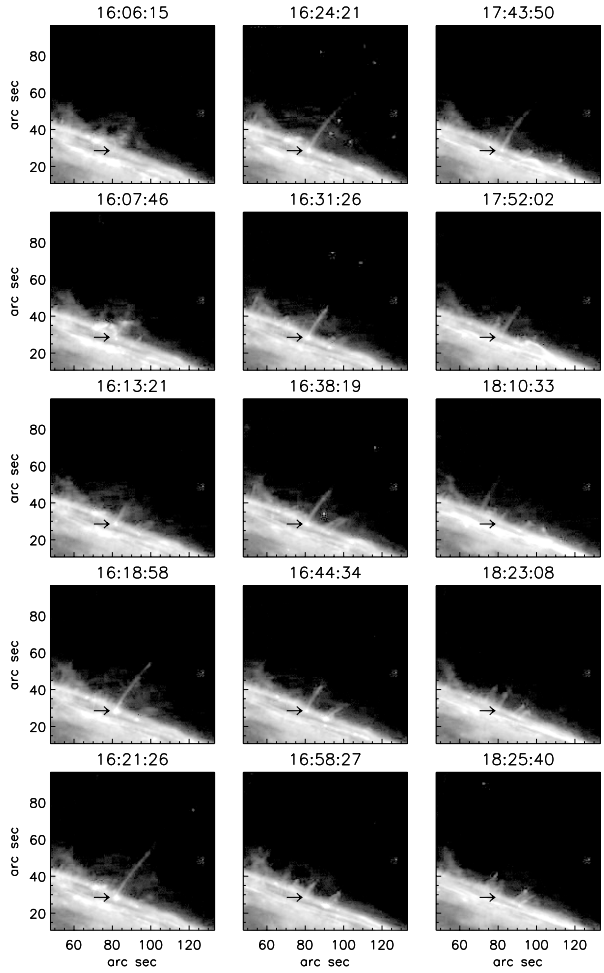

Fig. 5. TRACE 1600 Å images at selected times (time runs from top to bottom and from left to right). The black arrow points at the base of the surge. Plotted coordinates correspond to those of Fig. 4.

comparison of the DOT Ca II H and TRACE 195 Å images reveals that the EUV counterpart to the Ca II H surge is a dark absorption feature that intercepts the bright $\sim 10^6$ K background. The absorption mechanism is likely to be due to bound-free extinction by hydrogen and helium (Kucera et al. 1998; Rutten 1999), dominated by scattering rather than thermal destruction. Such bound-free scattering is not monochromatic because spontaneous recombination (the most likely process to follow radiative ionization) re-emits the absorbed photons preferentially near the ionization threshold. Each bound-free scattering sequence therefore not only redirects a 195 Å photon, but also shifts it out of the TRACE passband. The observed darkness therefore does not measure temperature even for thick structures.

4. Analysis and results

4.1. TRACE-DOT comparison of the surge

The longer duration and the larger field of view of the TRACE observations permit us to follow the evolution of the surge in the 1600 Å passband, where it is clearly visible. Figure 5 shows images of the appearance, development and decay of the surge at selected times. The surge starts with a sudden flare-like brightening near the limb at ~16:06 UT. It is very likely that the surge is the manifestation of the magnetic reconnection between new and pre-existing magnetic flux. If the new flux is due to newly emerging flux or to the reorganisation of local small scale magnetic fields cannot be proved or ruled out, since the magnetic topology cannot be examined, because the observed region is found nearly at the limb. The brightening at the base persists during the entire duration of the surge and is probably the non-resolved base of the inverted "Y" configuration clearly seen in the DOT images. After the appearance of the bright patch, a spiked jet extends upward and lasts for about two and a half hours (there is a gap in the observations between 17:20 and 17:42 UT). The surge has a strong recurrence tendency extending and shrinking at least 3 times during this observation period at apparently the same place. It repeatedly expands to heights up to 43 Mm (at ~16:24 UT) or 25 Mm (at ~16:38 UT) followed by intermittent retractions (e.g. at ~16:31 UT, ~16:58 UT). This behaviour can also be seen in Fig. 6. The apparent upward velocity is 90 km s^{-1}, although the rise phases of the surge do not exhibit a fairly steady extension of emission to higher altitudes. It is not clear if the decay phases are simply a reversal of the rise with retraction of the material moving to lower altitudes or an emission fading in the upper part of the structure. Finally, The surge starts shrinking at ~17:02 UT, is hardly visible at 18:23:08 UT, while at 18:25:40 UT is no more visible.

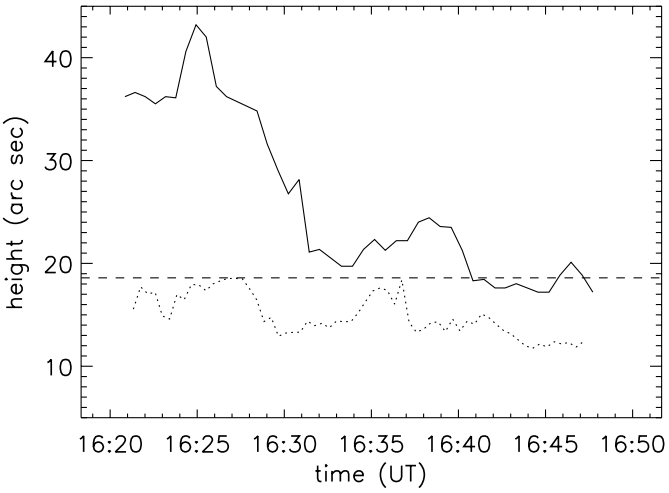

Fig. 6. Maximum height of the surge from TRACE 1600 Å images (solid line) and "apparent" Ca II H height of the surge (see text) from DOT images (dotted line). In both cases the height is measured from the base of the surge and its inclination has been taken into account. The dashed line shows the DOT FOV cutoff.

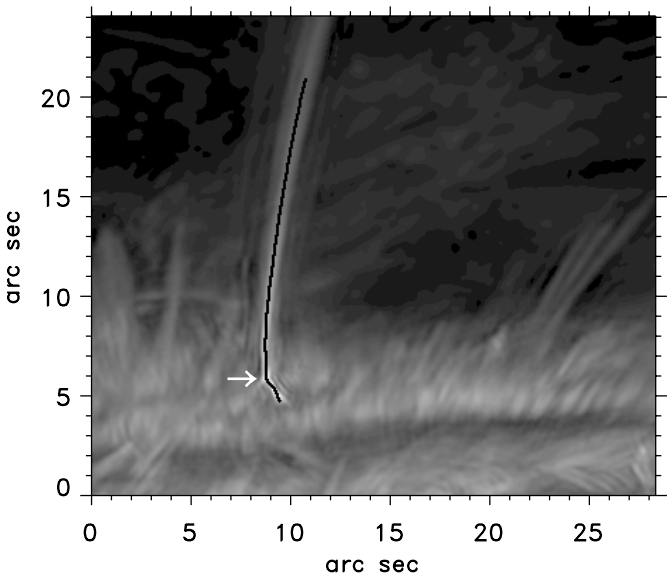

Fig. 7. Enlargement of the DOT observations of the surge area. The black solid line, superimposed on the surge, indicates the cut along the surge used for the time slice image of Fig. 8 and the spectral analysis described in 4.3. The white arrow indicates the mound-top of the inverted "Y" configuration which is also used as the origin for the apparent height calculation of Fig. 6.

The height of the surge in the 1600 Å TRACE images can be defined from the visible top of its intensity emission (see Fig. 5). In DOT images, the top of the surge is outside the field-of-view (FOV). However, an "apparent height" can be defined as the height where the Ca II H brightness inside the surge equals a specified value (brightness decreases as we move from the base of the loop upwards, see also Fig. 8). This value is chosen such that the maximum apparent height is always lower or equal to the DOT FOV cutoff. Figure 6 displays the measured 1600 Å height and the apparent Ca II H height of the surge. The lateral inclination was taken into account. The dashed line in Fig. 6 shows the DOT FOV cutoff. The origin for the height measurements is indicated by an arrow in Figs. 5 and 7 and coincides in the latter with the mound-top of the inverted "Y" configuration. The motion of the brightness fronts in both temporal sequences may not correspond to true material motion, if the emission fronts were to propagate at a rate different from that of the matter. However, the qualitatively good correspondence between the two curves suggests that both curves represent actual material motion. It seems also that there is a brief time delay between the two curves which is also indicative of an upward material motion.

4.2. Intensity profile of a cut along the surge

In Fig. 7 we present an enlarged cut-out of Fig. 1 around the surge area. The position, direction and length of the surge does not change significantly with time in our DOT FOV, however its brightness does change. We analyse the brightness variations along the central axis of the surge (time slice image), which is indicated by a black line in Fig. 7. This axis contains also the mound-top of the inverted "Y" configuration and its right leg. As we have already mentioned in Sect. 3 such a configuration is usually associated with magnetic reconnection. We have averaged the intensity over a strip extending 0.14″ on either side of the main axis, which is carefully traced on

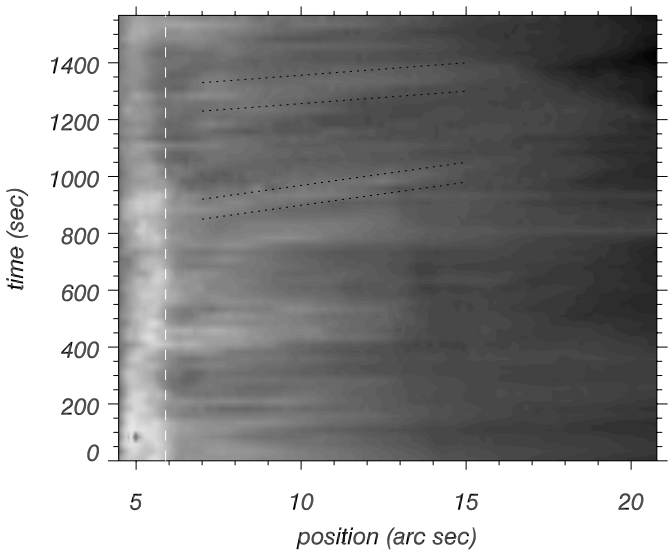

Fig. 8. Brightness along the main axis of the surge (see text and Fig. 7) as a function of position and time. The starting time corresponds to the beginning of the DOT observations at 16:21:20 UT, while position corresponds to the y-coordinates of the cut shown in Fig. 7. The vertical white dashed line indicates the mound-top of the inverted "Y" configuration. The black dotted lines frame two bright ridges indicating upward propagating disturbances.

all images of the time sequence as the position of maximum brightness at each height along the surge. This ensures taking into account small changes in the direction of the surge with time. Figure 8 shows the brightness along this cut against time. Several bright and dark ridges with respectively higher and lower brightness are visible which indicate the presence of propagating disturbances. The two clearest examples are the

brightness enhancements that start at positions $(x, t) = (6, 1250)$ and $(6, 900)$, framed within black dotted lines in Fig. 8. Positive gradients indicate upward travelling disturbances. By measuring the slope of each ridge we obtain apparent propagation speeds of 75 km s^{-1} and 50 km s^{-1}, respectively, for these two cases. Since these apparent speeds are associated with ridges that have the highest visible inclination, they represent a lower limit for propagation velocities along the surge. The obtained speeds far exceed the chromospheric sound speed of approximately 10–20 km s^{-1}. The upper brightness enhancement, with origin at $(x, t) = (6, 1250)$, stops suddenly at a height of $\sim 15''$. The dark wedge shape starting from that position around 1350 s may be due to impacted downward moving material returning back from above. The same wedge shape is visible for earlier brightness enhancements in Fig. 8. Another possibility is that the wedge shape maybe associated with actual variations of the length and hence brightness of the surge. The possibility that the material becomes optically thin near the top because of expansion cannot be excluded.

4.3. Spectral analysis

There is a hint for a periodic variation of the surge apparent Ca II H height in Fig. 6. Furthermore, the time slice image of Fig. 8 implies some kind of periodicity for the surge brightness. We are using a wavelet analysis to determine the presence and location of oscillations at the base and within the main body of the surge.

Wavelet analysis The wavelet analysis permits the determination of any periodic signal within a time series and how this period varies with time. We refer the reader to Torrence & Compo (1998) for a detailed description of the wavelet analysis and to Fludra (2001) for a comparison between wavelet and Fourier analysis results of the same signal. For the wavelet transform we use the Morlet wavelet, which consists of a plane wave modulated by a Gaussian. The cone of influence (hereafter COI) defines the region where effects of zero padding of a finite series become important. Hence periodicities in the COI are doubtful. The global power spectrum is the average of the wavelet power spectrum over time (comprising the whole range of our time series, i.e. inside and outside the COI regions) and is more or less equivalent to the Fourier analysis spectrum. The significance level of any detected period is determined by comparison of the power spectrum to the background noise spectrum, which in our case is assumed to be Poissonian. A significance level of 95% indicates a 5% probability that any significant power is caused by chance. A randomization test, where the significance of a detected period is calculated with respect to a finite number of random permutations of the observed time series, has been also applied as a more reliable approach. We refer the reader to Banerjee et al. (2001) and Tziotziou et al. (2004) for a detailed description of this method. This method can also be applied for the global spectrum. There is a 3.5% error, due to the finite number of permutations used (equal to 200) for the estimated probabilities. Only power peaks with a period lower than a maximum value, defined as the maximum period of the COI line (hereafter *cut-off period*), are considered for this randomization analysis.

Cross-wavelet spectrum and phase difference For finding the phase difference between two time series with a wavelet analysis, a cross-wavelet transform is needed. The cross-wavelet transform between two series X and Y with wavelet transforms $W_n^X(s)$ and $W_n^X(s)$ is defined as $W_n^{XY}(s) = W_n^X(s)W_n^{Y*}(s)$ where $W_n^{Y*}(s)$ is the complex conjugate of $W_n^Y(s)$ (Torrence & Compo 1998). From this complex cross-wavelet transform one can define the *cross-wavelet power* $|W_n^{XY}(s)|$ and the *phase difference* $\phi_n(s) = \tan^{-1}[\Im\{W_n^{XY}(s)\}/\Re\{W_n^{XY}(s)\}]$, where $\Re$ and $\Im$ are respectively the real and imaginary components of the transform. It can be shown that this phase difference is analogous to that of the Fourier analysis (Bloomfield et al. 2004). The global cross-wavelet power is the average of the cross-wavelet power spectrum over time. The global phase difference is the time average of the phase difference over the whole time range (inside and outside COI regions) with cross-power weighting as introduced by Lites & Chipman (1979). It is defined as the angle of the vector sum of all cross-powers over time with reference to the real axis. This way the cross-power amplitudes, which correspond to the complex vector lengths, act as weights in setting the slope of the summed vector and help to avoid wraparound errors (when angle values just above π are transformed into values just below -π, leading to erroneous $\Delta\phi$) that occur with straightforward averaging of individual phase differences. We can also define an error $\Delta\phi_{\rm global}(s)$ for the calculated global phase difference as the absolute deviation between the calculated global phase difference and the angle

$$\psi(s) = \left(\sum_n \left| W_n^{XY}(s) \right| \ \phi_n^2(s) / \sum_n \left| W_n^{XY}(s) \right| \right)^{1/2} \quad (1)$$

which represents the weighted sum over time (represented by the n index) of all individual phase differences $\phi_n(s)$ with the power (length of the complex vector) set as the weight function, since the large length complex vectors contribute more to the calculation of the global phase difference.

4.3.1. Wavelet analysis within the surge

In Figs. 9 and 10 we present a spectral analysis at positions $5.4''$ and $8.8''$ respectively (see Fig. 8). The former position corresponds to a point within the right leg of the inverted "Y" configuration (see Fig. 7), while the latter at a higher point within the surge well above the mound-top of the inverted "Y" configuration. In both figures there is clearly a ~400 s periodicity present with a high probability for the higher position and a reasonable one for the lower position. A part of its power lays within the COI and hence maybe subjected to edge-effects, however, its persistence over the whole time series though with a lower power for later times, indicates its physical importance. This period corresponds to the 6-min oscillations reported for other chromospheric structures such as fibrils, dark grains and mottles (Tziotziou et al. 2004; De Pontieu et al. 2003). Although the aforementioned structures are found in different magnetic

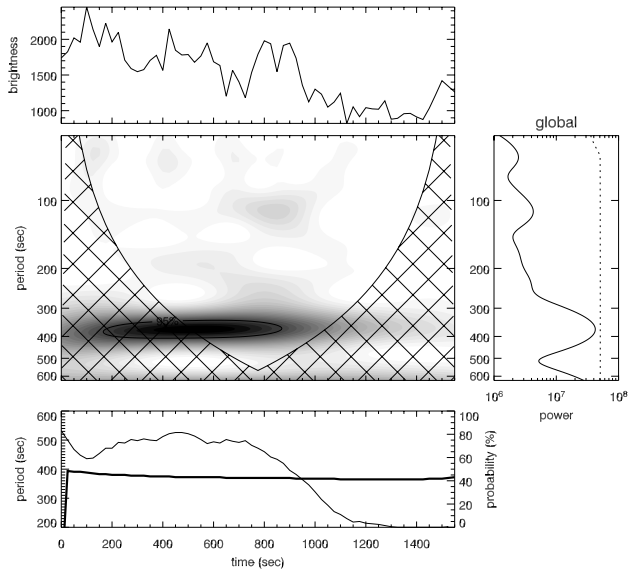

Fig. 9. Wavelet analysis of the brightness (in counts) of the surge at position 5.4″ (see Fig. 8). The middle left panel shows the time-period calculated power spectra for the brightness variations shown in the top panel with black representing high values of power (contours represent the significance level of 95%). Cross-hatched regions indicate the COI regions. The middle right panel shows the global power spectrum, i.e. the average of the wavelet power spectrum over time (the dotted line indicates the equivalent global significance level of 95%). The bottom panel shows the variations of the period (thick solid line) of the maximum power peak below the cut-off period (566 s) and its corresponding probability (thin solid line) obtained with the randomization method. There is a standard 3.5% error for the calculated probabilities. The global power spectrum shows a peak of 375 s with a corresponding global probability of 86%.

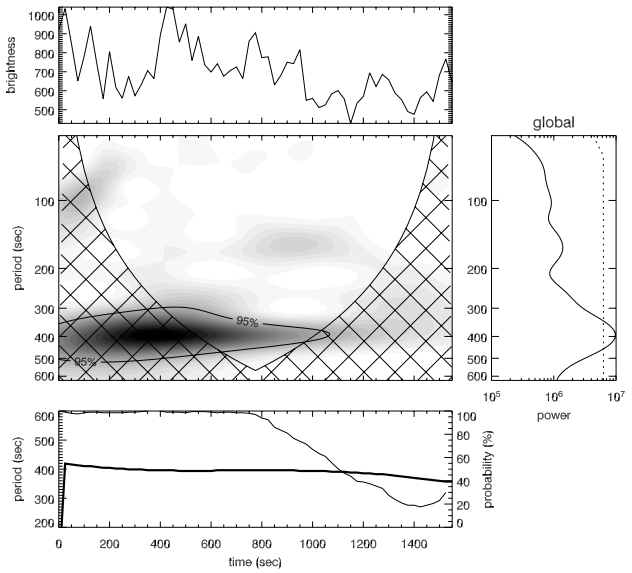

Fig. 10. Wavelet analysis of the brightness (in counts) of the surge at position 8.8″ (see Fig. 8). For a description of the presented panels see caption of Fig. 9. The cut-off period is 566 s. The global power spectrum shows a peak of 395 s with a corresponding global probability of 100%.

field topologies (quiet Sun for mottles and spicules, active regions for fibrils, dark grains and surges), the obtained same period suggests that probably all these structures have the same driving mechanism.

There is also a ∼120 s and a ∼180 s periodicity present in Figs. 9 and 10 respectively which could probably be related to the well-known 3-min chromospheric oscillation. However, both signals are rather week and hence insignificant.

In Fig. 11 (top panel) we present the phase difference derived from the cross-wavelet analysis between the brightness at the mound-top of the inverted "Y" configuration (dashed line in Fig. 8) and brightness at position 8.8″. White contours represent the logarithm of the corresponding cross-wavelet power. It is clear that the phase difference is smoothly and slightly changing (∼30°) over all periods between 350 and 450 s where the cross-wavelet power peaks exactly as in individual wavelet spectra (see Figs. 9 and 10). The same is observed for periods around 180 s, however with much less cross-wavelet power associated with it, while other periods show large variations, wraparounds, and small power and hence can be considered as noisy. In Fig. 11 (bottom panel) we present the corresponding global phase difference (solid line), calculated with cross-power weighting as described in Sect. 4.3, and its associated global cross-wavelet power (dashed line). We also show the calculated error range for the global phase difference as a surrounding grey area. It is clear that a) cross-power weighting corrects wraparounds and gives a smooth global phase difference as a function of period b) the errors for the global phase difference are large for periods lower than 350 s while for higher periods they are very small and c) the global cross-power spectrum for phase differences with periods other than ∼400 s is one or more orders of magnitude less and therefore the corresponding phase differences can not be considered so significant.

The same phase difference behaviour is found for almost all cross-wavelet spectra along the surge. We will further discuss results about phase differences along the surge in Sect. 4.3.2.

4.3.2. Wavelet analysis along the surge

Figure 12 shows the resulting global power spectra from a wavelet analysis of the brightness along the main axis of the surge (see Fig. 8). The oscillation with a ∼400 s periodicity is clearly visible for all heights except in the range of 12.8″ to 14.8″where other periods are more significant, probably because of noise in our data. The power is stronger below the mound-top of the inverted "Y" configuration and then reduces quickly beyond the height of 14″ probably due to decreased brightness. There is a trend of a slight increase of period with height with a local maximum also around the mound-top of the inverted "Y" configuration where reconnection is supposed to occur. It is interesting to note that the 3-min period signature, which is usually associated with the chromosphere, exists only very close to the base of the surge up to a height of ∼9″.

It is striking that both the lower part of the surge which is supposed to be related to magnetic reconnection and the higher part which is the product of this process are exhibiting similar period signatures, implying that the brightness variations

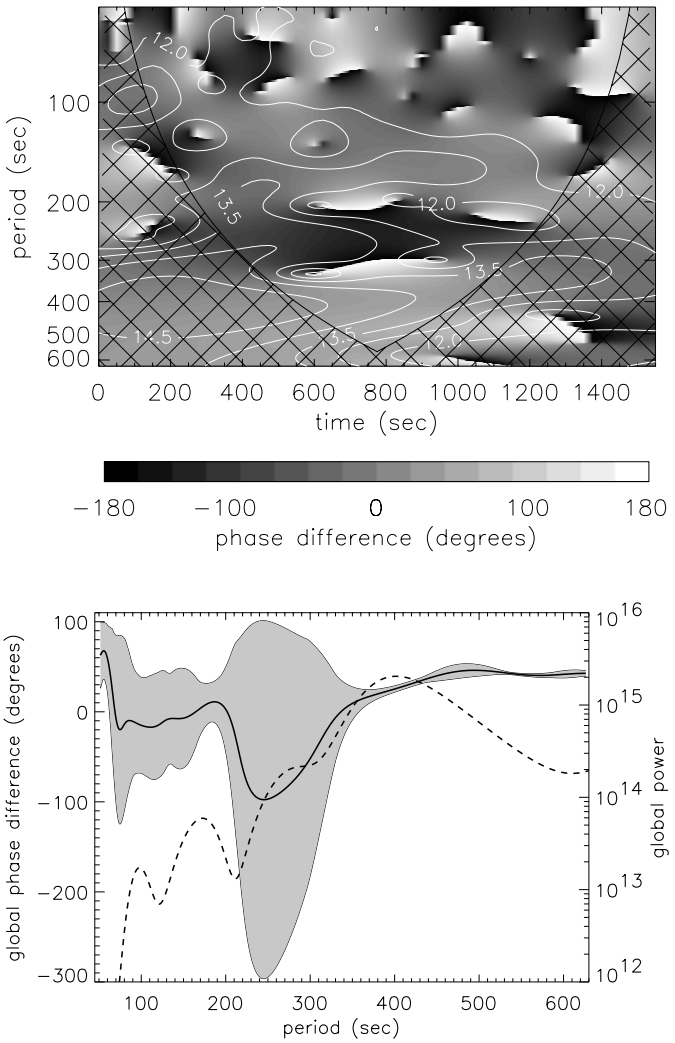

Fig. 11. *Top*: phase difference between brightness at the top of the inverted "Y" configuration (dashed line in Fig. 8) and brightness at position 8.8″. The cut-off period is 566 s. The overplotted white contours represent the logarithm of the cross-wavelet power. *Bottom*: the corresponding global phase difference (solid line) and the global cross-wavelet power (dashed line). The grey area denotes the error range for the global phase difference.

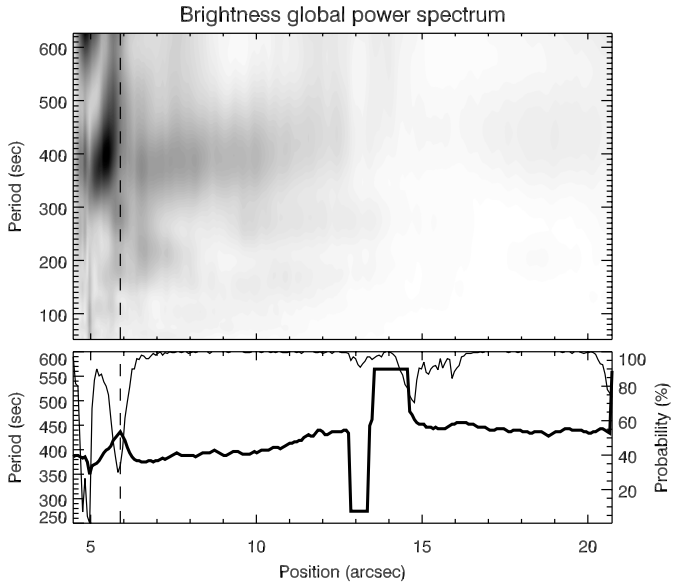

Fig. 12. Wavelet analysis results for the brightness along the main axis of the surge (see Fig. 8). *The top panel* shows the global power spectrum as a function of period and position along the axis of the surge. *The bottom panel* shows the variations of the period (thick solid line) of the maximum global power peak below the cut-off period (566 s) and its corresponding probability (thin solid line) obtained with the randomization method. There is a standard 3.5% error (see text) for the calculated probabilities. The vertical dashed line indicates the mound-top of the inverted "Y" configuration (see Figs. 7 and 8).

within the surge are strongly connected to its driving mechanism. If indeed reconnection is responsible for the creation of the surge, then it would push material upwards and downwards from the reconnection site leading to brightness variations along the surge.

In Fig. 13 we present the global phase difference as a function of position and period between the brightness at the top of the inverted "Y" configuration (dashed line in Fig. 8) and the brightness at each position along the main axis of the surge (see top panel of Fig. 11 for an example) as a function of position and period with overplotted contours of the logarithm of the corresponding global cross-wavelet power. In order to avoid wraparound errors along the position axis the global phase differences between neighboring positions were calculated and then added taking the top of the inverted "Y" configuration as reference position. This is why it runs from –280°to 150°. The figure clearly shows that there are only slight differences in the global phase difference behaviour as a function of position over the period range of 350 to 450 s, which is associated with the highest power almost at every position along the surge.

In Fig. 14 we present the global phase difference for a period of 400 s, as a function of position along the surge. This is the dominant period as also Fig. 12 demonstrates and its phase difference represents well the global behaviour over the period range of 350 to 450 s, as we have mentioned above. The grey area denotes the error range for the global phase difference. From this figure we can conclude that:

- Phase differences between the top of the inverted "Y" configuration, where reconnection is suggested to occur, and positions higher in the surge, are positive for the ranges 6″ to 9″ and 16″ to 21″ suggesting upward motion, and have very small errors. The phase difference becomes negative for positions 9″ to 16″, something impossible to explain with a plausible physical model. However, the associated errors are large and hence the global phase difference could well be positive as one would naturally expect. These large errors are probably due to noise, as also the period behaviour around these positions (Fig. 12, lower panel) clearly suggests.
- After positions 7.2″ and 19″ the upward motion seems to be decelerated. If this is indeed the case and the phase difference represents material motion then the higher velocity impacting material from below should cause shocks and hence brightness enhancements around these positions. Such brightenings are indeed observed within 7″ to 8″ in Fig. 8, quite clearly for times larger than 1000 s. However,

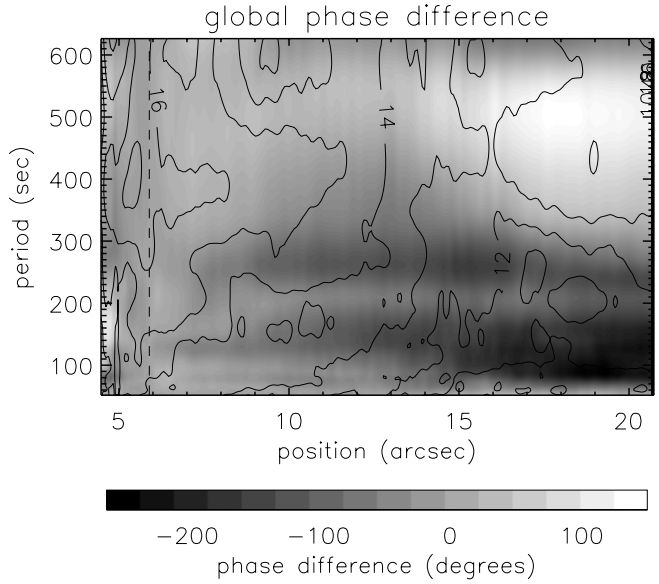

Fig. 13. Global phase difference as a function of period and position along the surge with overplotted contours of the logarithm of the corresponding global cross-wavelet power. The reference time series is the one corresponding to the top of the inverted "Y" configuration (vertical dashed line, see also Figs. 7 and 8). The cut-off period is 566 s.

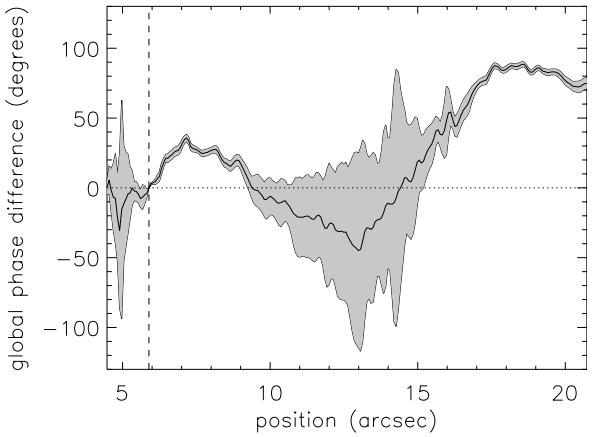

Fig. 14. Global phase difference (see text) for a period of 400 s as a function of position along the surge. The reference time series is the one corresponding to the top of the inverted "Y" configuration (vertical dashed line, see also Figs. 7 and 8). The grey area denotes the error range for the global phase difference. The cut-off period is 566 s.

no intensity brightenings are observed around 19″ probably due to the low intensity contrast.

– Phase differences between the top of the inverted "Y" configuration and positions below it, within the right leg of the surge, have large associated errors. If indeed magnetic reconnection is taking place, as the observed inverted "Y"-shape configuration at the base of the surge suggests, the outflowing material in both directions from the reconnection position should result to positive phase differences. This is indeed observed for the upward direction, however, what happens in the downward direction, within the right leg of the surge, is rather inconclusive due to large errors.

5. Discussion and conclusions

We have analysed high spatial and temporal resolution observations of the chromospheric limb observed with DOT and the dynamical characteristics of a surge observed both with DOT and TRACE.

In DOT images many tiny bright structures can been seen with a remarkable clarity protruding the limb as well as around the periphery of sunspot umbrae. Some of them, despite changes in brightness, are observed to persist for the whole time sequence, while others reappear several times at the same place in periods of a few minutes. The surge is a dynamic structure, shrinking and expanding several times at almost the same place. It can be followed for at least 2.5 h in TRACE images, showing rise velocities of ∼90 $\mathrm{km\,s^{-1}}$. It consists of relatively cold material of about 10^4 to 10^5 K.

Since surges are suggested to be driven by magnetic reconnection, its observed long lifetime indicates that the magnetic flux associated with the interacting opposite magnetic elements is not annihilated all at once, but continuously and steadily over a long period of time. Magnetic reconnection at the base of the surge is implied both by a) the observed inverted "Y"-shape configuration that fits the model picture of Kurokawa & Kawai (1993); b) the intensity brightening observed in the 1600 Å TRACE passband, which first manifests itself during the birth of the surge at its base and clearly persists during its whole lifetime; and c) the positive phase differences relative to the reconnection position in both upward and downward direction, suggesting, exactly as expected by reconnection models, outflowing material or waves from that position.

Applying a wavelet analysis in the high-cadence DOT observations we find brightness oscillations with a dominant ∼6 min periodicity at positions within and along the whole body of the surge. Oscillations with such a periodicity are not uncommon, and have been found for several other chromospheric structures, both in quiet (e.g. mottles) and active regions (e.g. fibrils, grains). We refer the reader to works by De Pontieu et al. (2003) and Tziotziou et al. (2004). The exact reason for this periodicity is not easily determined without a detailed study of the underlying magnetic field topology with high spatial resolution magnetograms, which are unfortunately not available for this study. However, this 6-min periodicity points strongly in the direction of a p-mode associated driver which has already been suggested by numerical simulations for fibrils by De Pontieu et al. (2004, 2005).

Apart from oscillations we also find outward propagating disturbances with different apparent propagation speeds, however clearly in excess of 50 $\mathrm{km\,s^{-1}}$. It is not absolutely clear whether these disturbances are related to bulk material motion or waves, since we are lacking line profiles that would permit us such a distinction through a detailed study of both velocity and intensity variations. However, there are some facts that are indicative of actual material motion. These are: a) the good correlation between the DOT and TRACE surge apparent heights shown in Fig. 6; b) the apparent brief time delay between the two height curves, and c) the phase difference behaviour along the surge and in particular the good correlation between the observed phase difference and the intensity behaviour

(i.e. brightenings due to shocks caused by impacts to slower moving material) as described in Sect. 4.3.2.

Some important key elements missing in the present study are a) observations in different wavelengths accompanied by high resolution magnetograms in order to associate features observed simultaneously at different temperatures, and to determine how the observed dynamics and oscillations are excited; and b) line profiles for the better distinction between material motion or wave propagation. The new extended capabilities of the DOT, which now permits the simultaneous recording of a $90'' \times 70''$ FOV in five different wavelength channels, one of which allows the recording of Hα profiles through a tunable filter, together with a future sixth camera for Ba II 4554 Å Dopplergrams and magnetograms, are very promising towards this direction.

Acknowledgements. The DOT is operated by Utrecht University at the Spanish Observatorio del Roque de los Muchachos of the Instituto de Astrofísica de Canarias and is presently funded by Utrecht University, the Netherlands Organisation for Scientific Research NWO, The Netherlands Graduate School for Astronomy NOVA, and SOZOU. Wavelet software was provided by C. Torrence and G. Compo and is available at `http://paos.colorado.edu/research/wavelets/`. We thank R. J. Rutten and A. G. de Wijn for many constructive discussions and comments. The DOT efforts and K. Tziotziou's research is funded by the European Commission through the European Solar Magnetism Network (contract HPRN-CT-2002-00313).

References

Banerjee, D., O'Shea, E., Doyle, J. G., & Goossens, M. 2001, A&A, 371, 1137
Bloomfield, D. S., McAteer, R. T. J., Lites, B. W., et al. 2004, ApJ, 617, 623
Bohlin, J. D., Vogel, J. D., Purcell, N. R., et al. 1975, ApJL, 197, L133
Canfield, R. C., Reardon, K. P. Leka, K. D., et al. 1996, ApJ, 464, 1016
De Pontieu, B., Erdélyi, R., & de Wijn, A. G. 2003, ApJ, 595, 63L
De Pontieu, B., Erdélyi, R., & James, S. P. 2004, Nature, 430, 536
De Pontieu, B., Erdélyi, R., & De Moortel, I. 2005, ApJ, 624, 61
Fludra, A. 2001, A&A, 368, 639
Foukal, P. 1971, Sol. Phys., 19, 59
Georgakilas, A. A., Koutchmy, S., & Christopoulou, E. B. 2001, A&A, 370, 273
Handy, B. N., Acton, L. W., Kankelborg, C. C., et al. 1999, Sol. Phys., 187, 229
Kucera, T. A., Andretta, V., & Poland, A. I. 1998, Sol. Phys., 183, 107
Kurokawa, H., & Kawai, G. 1993 in The Magnetic and Velocity Fields of Solar Active Regions, ed. H. Zirin, G. Ai, & H. Wang (San Francisco: ASP), ASP Conf. Ser., 46, 507
Leenarts, J., & Wedemeyer-Böhm, S. 2005, A&A, 431, 687
Lites, B. W., & Chipman, E. G. 1979, A&A, 231, 570
Roy, J.-R. 1973a, Sol. Phys. 28, 95
Roy, J.-R. 1973b, Sol. Phys. 32, 139
Rust, D. M. 1968, IAU Symp., 35, 77
Rutten, R. J. 1999, in Magnetic Fields and Oscillations, ed. B. Schmieder, A. Hofmann, & J. Staude, ASP Conf. Ser. 184, 181
Rutten, R. J., Hammerschlag, R. H., Bettonvil, F. C. M., Sütterlin, P., & de Wijn, A. G. 2004a, A&A, 413, 1183
Rutten, R. J., de Wijn, A. G., & Sütterlin, P. 2004b, A&A, 416, 333
Schmieder, B., Golub, L., & Antiochos, S. K. 1994, ApJ, 425, 326
Svestka, Z. 1976, Solar Flares (Dordrecht: Reidel)
Tandberg-Hanssen, E. 1977, in Illustrated Glossary for Solar and Solar-Terrestrial Physics, ed. A. Bruzek, & C. J. Durrant (Dordrecht: Reidel), 106
Torrence, C., & Compo, G. P. 1998, Bull. Amer. Meteor. Soc., 79, 61
Tziotziou, K., Tsiropoula, G., & Mein, P. 2004, A&A, 423, 1133
Yokoyama, T., & Shibata, K. 1996, PASJ, 48, 353
Yoshimura, K., Kurokawa, H., Shimojo, M., & Shine, R. 2003, PASJ, 55, 313